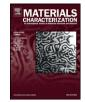
ELSEVIER



Contents lists available at ScienceDirect

## Materials Characterization

journal homepage: www.elsevier.com/locate/matchar

## Characterization of complex carbide-silicide precipitates in a Ni-Cr-Mo-Fe-Si alloy modified by welding



### D. Bhattacharyya \*, J. Davis, M. Drew, R.P. Harrison, L. Edwards

Institute of Materials Engineering, Australian Nuclear Science and Technology Organization, Lucas Heights, NSW 2234, Australia

#### A R T I C L E I N F O

#### ABSTRACT

Article history: Received 9 December 2014 Received in revised form 21 April 2015 Accepted 1 May 2015 Available online 5 May 2015

Keywords: Transmission electron microscopy Energy dispersive spectroscopy Focused ion beam Nickel based alloy Hastelloy-N Welding structures Nickel based alloys of the type Hastelloy-N<sup>™</sup> are ideal candidate materials for molten salt reactors, as well as for applications such as pressure vessels, due to their excellent resistance to creep, oxidation and corrosion. In this work, the authors have attempted to understand the effects of welding on the morphology, chemistry and crystal structure of the precipitates in the heat affected zone (HAZ) and the weld zone of a Ni–Cr–Mo–Fe–Si alloy similar to Hastelloy-N<sup>™</sup> in composition, by using characterization techniques such as scanning and transmission electron microscopy. Two plates of a Ni–Cr–Mo–Fe–Si alloy GH-3535 were welded together using a TiG welding process without filler material to achieve a joint with a curved molten zone with dendritic structure. It is evident that the primary precipitates have melted in the HAZ and re-solidified in a eutectic-like morphology, with a chemistry and crystal structure only slightly different from the pre-existing precipitates. In the molten zone, the primary precipitates were fully melted and dissolved in the matrix, and there was enrichment of Mo and Si in the dendrite boundaries after solidification, and re-precipitates in the molten zone varied according to the local chemical composition.

Crown Copyright © 2015 Published by Elsevier Inc. All rights reserved.

#### 1. Introduction

Among the high temperature alloys, nickel based alloys have been preferred in the power industry, in both the fossil fuel power plants and nuclear power reactors [1,2] (such as light-water reactors, LWR, pressurised water reactors, PWR, boiling water reactors, BWR, and molten-salt reactors, MSR). In general, because of their low void swelling characteristics [3,4], higher creep resistance than stainless steels [5] and high corrosion resistance [6], Ni based alloys are preferred candidate materials for Gen IV reactor in-core components where the temperatures encountered would be greater than 600 °C. Ni based alloys with Cr, Mo and Fe as major alloying elements, such as Hastelloy N™, are particularly suitable for molten salt reactors because of their high resistance to oxidation, corrosion and creep at elevated temperatures and molten salt environments [2,7,8]. The alloys frequently contain carbides of the form  $M_6C(\eta)$  and  $M_{23}C_6$  [7,9,10]. The Si content in these alloys not only improves oxidation resistance, but also stabilizes the complex silicide/carbide phases of the form Ni<sub>2</sub>(Mo,Cr)<sub>4</sub>(Si,C) and Ni<sub>3</sub>(Mo,Cr)<sub>3</sub>(Si,C) [7,11]. These phases appear in the form of equiaxed particles (with some faceting visible) in stringers parallel to the rolling or extrusion direction, and can be as large as 2–5 µm. It has been

E-mail address: dhb@ansto.gov.au (D. Bhattacharyya).

found that after welding, some non-equilibrium intermetallic phases such as  $\sigma$ , P and  $\mu$  may be formed due to rapid cooling and segregation [12–14]. In some cases, annealing at high temperatures, i.e., >1300 °C, has also been seen to cause the transformation of these complex silicide–carbides to an intermetallic  $\delta$  (Ni,Mo) phase [7]. An understanding of the evolution of the crystal structure, chemistry and morphology of these various types of precipitates during welding is of primary importance as they have been known to affect the ductility and fracture behaviour of this class of Ni based alloys. Although there have been some detailed studies of the nature of the precipitates and their stability after heat treatment [7,15–17], very few in-depth studies appear in the literature characterizing different types of precipitates in different weldment regions of this type of alloy. In the study by Ojo et al. [18], the authors characterize the microstructure of dendrites and precipitates in the weld fusion zone of IN 738LC alloy, while Unfried-Silgado et al. also focuses their attention on the microstructure of matrix and precipitates in the welded zone of Ni-Cr-Fe alloy with and without Mo additions [19] In this paper, the authors have attempted to characterize the precipitates as they appear in various locations in the welded sample, such as the HAZ or weld metal, using advanced sampling techniques such as focussed ion beam (FIB) milling to extract site-specific samples for transmission electron microscopy (TEM). The information thus obtained has been complemented with advanced characterization techniques such as high-resolution energy dispersive spectroscopy (EDS) and electron backscatter diffraction (EBSD) to gain a deeper

<sup>\*</sup> Corresponding author at: Bldg. 3, Institute of Materials Engineering, ANSTO, New Illawarra Road, Lucas Heights, NSW 2234, Australia.

insight into the evolution of these precipitates as a function of the maximum local temperature reached during welding. This method of extracting samples from different parts of the cross-section of a welded specimen provides a unique opportunity for studying the effect of heating to a range of temperatures in a single sample, and has been found very useful by the authors here in getting a wide view of the various types of phase transformations occurring during the welding process.

#### 2. Experimental methods

The material used for the welding experiment was a piece cut from an extruded and solution annealed bar of Ni based alloy with the nominal composition close to that of Hastelloy® N, obtained from the Shanghai Institute of Applied Physics (SINAP). The chemical composition was determined by the LECO combustion method and inductively coupled plasma atomic emission spectroscopy (ICP-AES), and is given (in wt.%) in Table 1 below.

Two pieces were cut from the rod of diameter approximately 17 mm (Fig. 1(a)), and welded together in the manner shown in Fig. 1(b), using a tungsten inert gas (TIG) weld, without any filler. The top piece and the bottom piece were rotated 90° with respect to each other before the welding, as shown in Fig. 1(c). The welding was performed at a current of 56 A at 9.9 V. The dimensions of the welded pieces are shown in the figure. The process of welding caused the alloy in the top part to melt and flow downwards, and subsequently solidify in the curved shape, as shown schematically in Fig. 1(d) and (e).

A cross-section of the weld was cut and mounted in a conductive Bakelite mould, and polished to SEM quality finish (better than 0.05 µm). The sample was characterized using a Zeiss® Ultra Plus™ scanning electron microscope (SEM) to examine the microstructure, and orientation maps were obtained using electron backscatter diffraction method (EBSD). The chemical composition of the various phases was obtained in the SEM using energy dispersive X-ray spectrometry. EBSD and EDS analysis were done using the HKL<sup>™</sup> and AZTEC<sup>™</sup> software and detectors manufactured by Oxford Instruments<sup>™</sup>. When some pixels were un-indexed in the EBSD maps, these were "cleaned up" based on the orientation of the surrounding pixels using the "Cleanup" procedure in HKL® Tango<sup>™</sup>. The un-indexed pixels were replaced only when they had a minimum of 7 indexed neighbours (out of a possible 9).

Samples for cross-sectional transmission electron microscopy (TEM) from specific areas in the weld, HAZ and base metal were obtained using a Zeiss® Auriga<sup>™</sup> focused ion beam (FIB) instrument, with a Cross-beam<sup>™</sup> configuration. These samples were first cut out using relatively high accelerating voltage for the Ga ions (30 kV), and high currents (>600 pA). They were then thinned to electron transparency using lower voltages (2–5 kV), and lower currents (100–240 pA), to try to minimize the damage caused by Ga ion implantation and collision cascades. The samples were then examined using a Jeol® 2200 FS<sup>™</sup> and a Jeol® 2010 F<sup>™</sup> 200 keV TEM. The structure of the precipitates and the matrix was determined using selected area diffraction techniques, and the chemical composition by energy dispersive X-ray spectrometry (EDXS) using an Oxford Instruments® EDS detector.

Differential thermal analysis (DTA) [20] was performed in order to determine the melting point of the alloy and of any of the minor phases, using a Seiko® DTA/TGA instrument. The sample was heated in an Ar atmosphere at ~20 °C/min to ~1468 °C and held at this temperature for 1 min, and cooled at ~100 °C/min to about 1200 °C. The furnace was

ladie I	
Chemical composition of the Ni-Mo-Cr-Fe alloy in wt	.%.

T-1-1- 4

Мо	Cr	Fe	Mn	Si	Al	С	Ni
16.0	6.40	3.62	0.58	0.43	0.06	0.05	Bal

subsequently switched off and the sample allowed cooling to room temperature within the furnace.

#### 3. Results

#### 3.1. Preliminary characterization of the weld microstructure

An SEM backscatter image of the cross-section of the weld is shown in Fig. 2(a). It is clear from this image that the weld metal spread out in a curved manner due to gravitational force and resolidified in long dendritic structures. The dashed line in the image gives the approximate fusion line boundary between the weld metal and the heat affected zone (HAZ). The EBSD generated grain boundary map in Fig. 2(b) shows the random high angle grain boundaries in black and the  $\Sigma$ 3 twin boundaries in green. It is clear that in the melt zone, the material did not form any twins in the dendritic grains formed after resolidification. In fact, there is a clear distinction between the dendritic grains in the weld zone on the one hand and the grains in the HAZ and the parent metal on the other, in that almost all twin boundaries appear in the base metal/HAZ grains, and almost none appear in the weld zone. This fact, along with the shape of the grains, can be used as a very good guideline to demarcate the weld fusion boundary.

The SEM image in Fig. 3(a) shows a magnified view of the region near the boundary of the weld metal and base metal, with the weld joint between the two bars going horizontally, and the stringers of primary precipitates on the upper left side of the weld line, which were present in the as received material. The precipitates do not appear in stringers in the lower bar below the weld joint, because the lower piece was rotated 90° with respect to the upper piece prior to welding, and therefore, the section shown here is cut transverse to the direction of the stringers for the lower part of the sample. This situation is shown schematically in Fig. 1(c). The precipitates constituting the stringers are more or less equiaxed in general, with the size in the range of  $1-5 \,\mu\text{m}$ , and are slightly faceted, as shown in Fig. 3(b). As is evident from Fig. 3(a), the pre-existing precipitates melted and dissolved in the weld metal, and the stringers are no longer visible in the re-solidified dendritic grains. However, newly formed fine precipitates are visible in the weld metal, which are shown more clearly in the high magnification image in Fig. 3(c), where the distribution of these precipitates along the dendrite boundaries is apparent. As can be seen from a careful observation of this image, the boundaries between two dendritic columns or lamellae in the same dendrite colony have segregation of solute (which was confirmed to be mostly Mo and Si by EDS, not shown here), whereas most of the precipitation occurred in the dendrite boundary triple points. The image in Fig. 3(d) shows the structure of one of these newly formed precipitates in detail, and it is clear that these precipitates have a eutectic-like morphology. There are also traces of diffusion of elements between the matrix and the eutectic like precipitates, visible in the upper part of the image.

In the heat affected zone (HAZ), i.e., within a band of about 150 µm of the fusion line, the pre-existing precipitates - which were almost equiaxed - are transformed to a new kind of precipitate, which also has a eutectic-like morphology. The image in Fig. 4(a) shows a row of precipitates forming a stringer, running from left to right in the image. The left part of the image is comprised mainly of the base metal, which may have experienced some increase in temperature, but not large enough to cause any significant amount of phase transformation. Thus we see almost unchanged precipitates in this area. As we move to the right, the maximum temperature reached is higher. One of the precipitates which was part of an original stringer is marked as 1, and is shown in a higher magnification image in Fig. 4(b). This precipitate has started to show some melting and re-solidification at the grain boundary, and possibly even some internal redistribution of elements, as is indicated by the network like pattern of brighter "strings". On moving further to the right, the temperature increases even more, and the pre-existing globular precipitates are replaced by a new kind of Download English Version:

# https://daneshyari.com/en/article/1570861

Download Persian Version:

https://daneshyari.com/article/1570861

Daneshyari.com